Acta Cryst. (1996). A**52**, 397–407

The Two-Channel Maximum-Entropy Method Applied to the Charge Density of a Molecular Crystal: α-Glycine

R. J. PAPOULAR,[a,b] Y. VEKHTER[c] AND P. COPPENS[c]*

[a]*Physics Department, Brookhaven National Laboratory, Upton, NY 11973, USA,* [b]*Laboratoire Léon Brillouin, CE de Saclay, 91191 Gif-sur-Yvette, France, and* [c]*Department of Chemistry, Natural Science & Mathematics Complex, State University of New York at Buffalo, Buffalo, NY 14260, USA. E-mail: che9990@ubvms.cc.buffalo.edu*

(*Received 5 July 1995; accepted 19 December 1995*)

Abstract

A two-channel maximum-entropy method (MEM), first used to enhance magnetization densities from phased polarized neutron data by Papoular & Gillon [(1990). *Europhys. Lett.* **13**, 429–434], has been applied to the electron deformation density. The resulting entropic densities are compared with standard deformation densities and with dynamic and static deformation maps obtained from multipole refinements. The procedure is illustrated with simulated and real single-crystal X-ray data sets on the molecular crystal of α-glycine. Both a uniform prior and a prior equal to the MEM-enhanced dynamic model deformation density are used in the MEM procedure, the result of which does not depend on the starting density. The method is judged by the appearance of the resulting maps and the values of the molecular dipole moment before and after the MEM. Compared with the conventional deformation density, the MEM procedure sharpens the peaks in the bond but flattens the weaker features, especially when a uniform prior is used. The dipole-moment criterion shows the non-uniform prior to be preferable to the uniform prior in reproducing electrostatic properties. The usefulness of the MEM in charge-density analysis remains open to discussion.

1. Introduction

The mapping of the electron distribution in molecules and crystals from diffraction data has been a topic of interest for the last 30 years. One of the main aims of such studies is the evaluation of electrostatic properties, based on the direct use of the measured structure factors $F(\mathbf{H})$, as originally proposed by Bertaut (1978), or in direct space from parameters obtained with aspherical atom models (Su & Coppens, 1992).

The maximum-entropy method has been proposed as the method of choice for enhancement of the electron density beyond the experimental resolution (Sakata & Sato, 1990; Sakata, Uno, Takata & Howard, 1993) and would thus appear the method of choice to optimize the information that can be extracted from an experimental data set and to produce the least possible biased density. Diffraction techniques make wide use of Fourier syntheses to obtain model-free information about various scattering densities from sparse and noisy sets of structure factors, provided that the latter are suitably phased. As is well known, Fourier syntheses are subject to truncation errors and other effects owing to incompleteness of the data set. It is precisely in this context of image processing that maximum entropy (MaxEnt) was first successfully applied in astronomy by Frieden (1972) and Gull & Daniell (1978). The phases are assumed to be reliably known from a reasonable model or from the experiment itself.

The relevance of MaxEnt to crystallography was stressed by Collins (1982), Livesey & Skilling (1985) and others. Its application has spread with the advent of nonlinear efficient algorithms (Bricogne, 1984; Skilling & Bryan, 1984; Skilling & Gull, 1985) and dedicated crystallographic programs such as *MEED* (Sakata & Sato, 1990; Kumazawa, Kubota, Takata, Sakata & Ishibashi, 1993). However, it has been recently pointed out by Jauch & Palmer (1993) and Jauch (1994) that MaxEnt is of little use when the densities to be reconstructed have a large dynamic range and the aim is to recover fine and detailed information. This is very much the case when bonding effects are to be studied, in which case the deviations from sphericity of the electron distribution about the nuclei are relatively small for all but the H atoms.

Use of a difference method reduces the dynamic range of the reconstruction substantially, such that minor features become relatively more pronounced. The deformation density $\Delta\rho(\mathbf{r}) = \rho(\mathbf{r}) - \rho_{\rm ref}(\mathbf{r})$ is an appropriate function for such a method. The retrieval of both the positive $\rho^+(\mathbf{r})$ and the negative $\rho^-(\mathbf{r})$ parts of the deformation density, $\Delta\rho(\mathbf{r}) = \rho(\mathbf{r}) - \rho_{\rm ref}(\mathbf{r}) = \rho^+(\mathbf{r}) - \rho^-(\mathbf{r})$, requires the use of a two-channel entropy formalism. The latter has been shown to be quite useful in the context of magnetization densities (Papoular & Gillon, 1990*a*,*b*) and of unpolarized neutron diffraction involving atoms with scattering lengths of opposite signs (Sakata *et al.*, 1993). The use of a multichannel approach in the analysis of crystal structures in which the spatial

distribution is different for different atoms has been discussed by Bricogne (1988).

As a test case, we have selected a low-temperature experimental single-crystal X-ray data set on the small-unit-cell crystal of α-glycine by Legros & Kvick (1980). The crystal is monoclinic, centrosymmetric, space group $P2_1/n$, and the X-ray data span the range $\sin\theta/\lambda = 0.00$–$1.20\ \text{Å}^{-1}$, with 1205 reflections for which $F > 2\sigma(F)$.

2. The single-channel MaxEnt method and its shortcomings in the reconstruction of details of the electron-density distribution

The Cambridge MaxEnt algorithm (Skilling & Bryan, 1984; Gull & Skilling, 1991) is used in the analysis. Its application to a phased set of diffraction data essentially follows the approach of Collins (1982). Crystallographic symmetry is forced into the density reconstructions using the averaged Fourier coefficients introduced by Papoular (1991). No use is made of fast Fourier transform methods. For the single-channel method, the value of $F(\mathbf{0})$ was not included in the data set.

The retrieval of the positive charge density $\rho(\mathbf{r})$ in a crystal from a limited and noisy set of N unique structure factors $F^{\text{obs}}(\mathbf{H}_k)$ and their related e.s.d. bars $\sigma(\mathbf{H}_k)$ is a problem for which MaxEnt is well suited. The first step is to digitize the unit cell (or a suitable subunit) of volume V into M pixels of size $\Delta = V/M$, at the centers $\mathbf{r}_j$ of which the density values $\rho_j = \rho(\mathbf{r}_j)$ are sought. The second step is to maximize the discrete entropy functional

$$S[\rho(\mathbf{r})] = -\sum_{j=1}^{M} p(\mathbf{r}_j)\ln[p(\mathbf{r}_j)/m(\mathbf{r}_j)], \tag{1}$$

where $p(\mathbf{r}_j)$, the probability of the density associated with pixel j, and the corresponding probability $m(\mathbf{r}_j)$ for the prior (model) density $\rho_0(\mathbf{r})$ are defined as

$$p(\mathbf{r}_j) = p_j = \rho(\mathbf{r}_j)\Big/\sum_{j=1}^{M}\rho(\mathbf{r}_j),$$
$$m(\mathbf{r}_j) = m_j = \rho_0(\mathbf{r}_j)\Big/\sum_{j=1}^{M}\rho_0(\mathbf{r}_j). \tag{2}$$

The entropy functional $S[\rho(\mathbf{r})]$ is maximized subject to the constraint $C[\rho(\mathbf{r})] = \chi^2 = N$, the number of unique structure factors, where

$$C[\rho(\mathbf{r})] = \chi^2 = \sum_{k=1}^{N} |[F^{\text{obs}}(\mathbf{H}_k) - F^{\text{calc}}(\mathbf{H}_k)]|^2/\sigma(\mathbf{H}_k) \tag{3a}$$

and

$$F^{\text{calc}}(\mathbf{H}_k) = (V_{\text{unit cell}}/M)\sum_{j=1}^{M}\rho(\mathbf{r}_j)\exp\{2\pi i\mathbf{H}_k\cdot\mathbf{r}_j\} \tag{3b}$$

with suitable scaling to F^{obs}.

Note that (3*b*) remains valid when only a subunit of the unit cell is digitized into M pixels, provided that this subunit remains a multiple of the asymmetric unit.

Maximizing $S[\rho]$ with respect to the ρ_j's under constraint requires the use of a Lagrange multiplier λ. As first described by Skilling & Bryan (1984), the Lagrangian functional $L = S - \lambda\chi^2$ is introduced, where $S = S[\rho(\mathbf{r})]$. At convergence,

$$\nabla_\rho(L) = \nabla_\rho(S) - \lambda\nabla_\rho(\chi^2) = 0. \tag{4a}$$

In the case of a uniform prior, $\rho_0(\mathbf{r}_j) = \rho_{0j} = \rho_0$ for all j and condition (4*a*) is conveniently recast into

$$\rho_j = A\exp\{-\lambda(\textstyle\sum\rho_j)\partial C[\rho]/\partial\rho_j\}, \tag{4b}$$

where

$$A = \exp\{\textstyle\sum p_j\ln\rho_j\}. \tag{4c}$$

The quantity A is thus a weighted logarithmic average of the converged entropic density $\rho(\mathbf{r})$ over the unit cell.

The algorithm is non-linear, iterative and solves for both $\lambda(n+1)$ and $\rho_j(n+1)$ starting from $\lambda(n)$ and $\rho_j(n)$ at iteration n. The starting ($n = 0$) values are $\lambda \simeq 0$ and $\rho_j(0)$ as defined by the prior density. Achieving convergence involves a two-step process, in which first the $\chi^2 = N$ constraint is satisfied and subsequently the entropy S is maximized.

Both C and S are expanded quadratically and the search for $\rho_j(n)$ replaced by a search for increments $\delta\rho_j(n)$. An additional distance penalty function is introduced to make sure that the increments $\delta\rho_j(n)$ do not become too large. From (4*b*), suitably modified to allow for the penalty function just mentioned, $\rho_j(n+1)$ is expressed as a function of $\rho_j(n)$ and $\lambda(n+1)$. The latter $\lambda(n+1)$ value, unknown at this point, is found by satisfying the constraint $C[\rho(n+1)] = N$. $\rho_j(n+1)$ is then derived.

When used with limited data sets of ten or twenty unique structure factors, the non-linear iterative MaxEnt algorithm is rather insensitive to the tunable parameter A. By contrast, the use of large data sets requires a careful tuning of this parameter. In practice, A is assigned a given starting value and the MaxEnt algorithm is run iteratively until convergence is obtained and the constraint $\chi^2 = N$ is met. It can be shown that the extrapolated entropic value of $F(\mathbf{0})$ increases monotonically with A. It is seen from (4*b*) that the expected density far away from any atom is of the order A, since $\partial C[\rho]/\partial\rho_j$ is then expected to be negligible. Hence, A should be kept as small as possible. On the other hand, A increases with the dynamic range of the density as implied by (4*c*). As enlarging the data set by incorporating more measured Bragg peaks to achieve higher spatial resolution will increase the amount of structure in the reconstruction, it will also increase A, in which intense features are more heavily weighted. Consequently, there is a loss of sensitivity to weak density features. If A is too

small, the algorithm never reaches convergence or produces a spuriously distorted density. If too large, it never converges. Reconstructed density values smaller than A are unreliable. A practical example of tuning A can be found in Papoular, Prandl & Schiebel (1992).

2.1. *Application to a simulated data set*

An upgraded version of the program *MOLLY* (Hansen & Coppens, 1978), *LSMOL*90, was used in a multipolar refinement of the experimental data on the α-glycine data set of Legros & Kvick (1980). The positional and thermal parameters of the C, N, O and H atoms, the κ parameters and the multipole populations were varied in the least-squares refinement. The thermally averaged promolecule density was used to yield a set of 1205 simulated structure factors $F_{\rm sph}(\mathbf{H})$, to which the experimental standard deviations were assigned.

The asymmetric unit of the crystal was defined as the region with $0 < x < 1$; $0 < y < 1/4$, $0 < z < 1$ [$a = 5.084\,(1)$, $b = 11.820\,(2)$, $c = 5.458\,(1)$ Å, $\beta = 111.95\,(2)°$], and divided into $32 \times 16 \times 32$ pixels. An everywhere-positive three-dimensional density reconstruction was carried out, using a uniform prior density. An optimal value of the default density $A = 1.82\,\text{e Å}^{-3}$ was found as follows. First, a very small value of A, $0.01\,\text{e Å}^{-3}$, was selected. After each iteration, n, of the *MaxEnt* algorithm, yielding current values of the density $\rho_j^{(n)}$, this value was upgraded to $A^{(n)} = \exp \sum_j p_j^{(n)} \ln \rho_j^{(n)}$ until $\chi^2 = N = 1205$, which was reached after 160 iterations. Because $F(\mathbf{0})$ is not used as a data point, this process diverges and the density increases indefinitely. The algorithm was subsequently run with the constant default value $A = A^{(160)} = 1.82\,\text{e Å}^{-3}$ until convergence, requiring a few more iterations. The value of the reconstructed density far from the atoms is already small, and A could probably be reduced down to about $1.5\,\text{e Å}^{-3}$, but this would not affect our discussion. The resulting O(1)—C(1)—O(2), N—C(2)—C(1) and N—H(1)···O(1) sections are shown in Fig. 1. The main features, the spherical density representing the C, O and N atoms, are reconstructed as such, but the density at the H-atom site is significantly flattened. The highest value of the density in the section, $38\,\text{e Å}^{-3}$, is found at the O-atom sites. The lowest level drawn ($2\,\text{e Å}^{-3}$) is clearly not physically significant.

Since the MaxEnt algorithm is intrinsically non-linear, and hence iterative, we examined the influence of using two very distinct starting densities on the final converged charge density. The first starting density is obtained from the 1205 $F_{\rm sph}$ Fourier coefficients. Those pixels corresponding to negative or zero values of the Fourier density are assigned an identical very small positive value instead. The second starting density is the flat uniform density, with a value chosen equal to A, the default density. Both choices result in two virtually indistinguishable entropic solutions within $A = 1.82\,\text{e Å}^{-3}$, our sensitivity level.

Since the sensitivity level is much larger than the effects to be found in the deformation electron density, which are typically less than $1\,\text{e Å}^{-3}$, an alternative procedure is called for.

3. The two-channel method for retrieval of the deformation electron density

3.1. *The two-channel entropy $S[\Delta\rho(\mathbf{r})]$*

As the wide dynamic range involved in the total electron density $\rho(\mathbf{r})$ interferes with the retrieval of the relatively weak features of chemical interest, for better sensitivity the analysis may be performed on the deformation $\Delta\rho(\mathbf{r})$, which has a much smaller dynamic range. The deformation density and the deformation structure factors are defined by

$$\Delta\rho(\mathbf{r}) = k\rho^{\rm total}(\mathbf{r}) - \rho^{\rm sph}(\mathbf{r}) \tag{5a}$$

$$\Delta F(\mathbf{H}) = kF^{\rm total}(\mathbf{H}) - F^{\rm sph}(\mathbf{r}), \tag{5b}$$

where k is a scale factor relating the experimental and absolute scales. The optimal value of k is further discussed below.

The local difference density $\Delta\rho(\mathbf{r})$ can be either positive or negative. Its average over the unit cell must be zero, since bonding effects only redistribute the electron density. Since the spherical part of the density is much larger than the deformation density, the phases of $F(\mathbf{H})$ are close, though not identical, to those of $F^{\rm sph}(\mathbf{H})$. For a centrosymmetric crystal, sign changes generally only occur for some extremely weak reflections.

The entropy functional $S[\rho(\mathbf{r})]$ defined by (1) requires a positive density everywhere in the unit cell. The associated probability $p(\mathbf{r})$ is proportional to the probability of finding an electron at $\mathbf{r}$. In the two-channel method, $\Delta\rho(\mathbf{r})$ is defined as the difference between two positive functions, $\rho^+(\mathbf{r})$ and $\rho^-(\mathbf{r})$, representing the densities of excess and lack of electrons, respectively. At a given $\mathbf{r}_j$ in the unit cell, either one or the other is significant since excess- and lack-of-electron densities are mutually exclusive. The related $p^+(\mathbf{r}_j)$ and $p^-(\mathbf{r}_j)$, defined as

$$p^+(\mathbf{r}_j) = \rho^+(\mathbf{r}_j)/\sum\{\rho^+(\mathbf{r}_j) + \rho^-(\mathbf{r}_j)\}$$

and (6)

$$p^-(\mathbf{r}_j) = \rho^-(\mathbf{r}_j)/\sum\{\rho^+(\mathbf{r}_j) + \rho^-(\mathbf{r}_j)\},$$

are the associated probabilities of finding either excess- or lack-of-electron density at $\mathbf{r}_j$. In analogy to the procedure used in the single-channel entropy method, the prior models $m^+(\mathbf{r})$ and $m^-(\mathbf{r})$ are introduced.

In analogy to (1), the two-channel entropy is defined as

$$S[\Delta\rho] = -\sum_{j=1}^{M}\{p_j^+ \ln(p_j^+/m_j^+) + p_j^- \ln(p_j^-/m_j^-)\}, \quad (7)$$

which quantifies the amount of structure present in a given deformation density $\Delta\rho(\mathbf{r})$.

We have followed two different approaches. In the first, the models $m^+(\mathbf{r}_j)$ and $m^-(\mathbf{r}_j)$ were taken to be uniform and equal across the unit cell; in the second approach, a non-uniform model based on the best prior guess for a chemically meaningful deformation density was used. The entropy-maximized dynamic deformation density from the least-squares multipole model was used as the model in the latter case. As an alternative, the theoretical deformation density could be taken.

The N diference structure factors are derived with $\Delta F^{\text{obs}}(\mathbf{H}_i) = kF^{\text{obs}}(\mathbf{H}_i) - F^{\text{sph}}(\mathbf{H}_i)$ values ($i = 1, N$) and the experimental standard deviations $\sigma(\mathbf{H}_i)$ are assigned to the difference structure factors. To maintain neutrality, $\Delta F(\mathbf{0})$ is added to the data set with a value equal to zero and a standard deviation five times less than the smallest

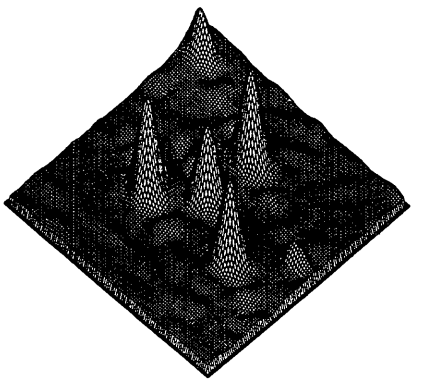

C1-O1-O2 plane: Standard FOURIER

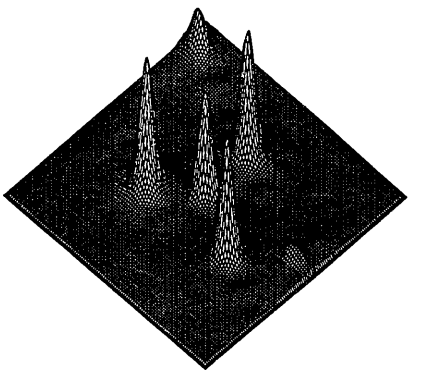

C1-O1-O2 plane: MAXIMUM ENTROPY

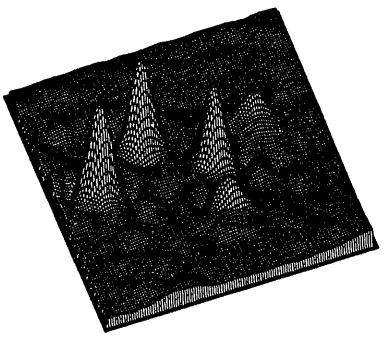

N-C1-C2 plane: Standard FOURIER

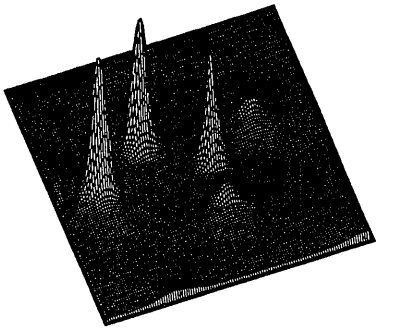

N-C1-C2 plane: MAXIMUM ENTROPY

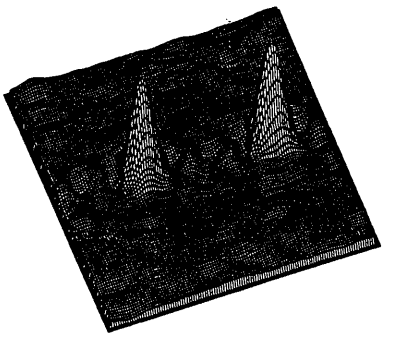

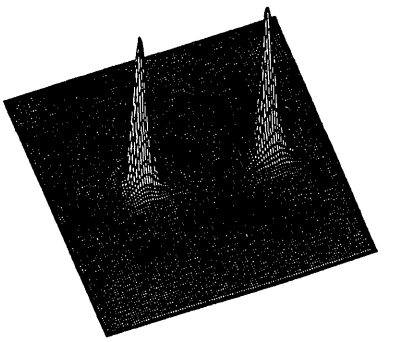

N-H1-O1 plane: Standard FOURIER N-H1-O1 plane: MAXIMUM ENTROPY

Fig. 1. Electron-density sections from the single-channel MEM procedure compared with the standard Fourier summation. Note the flattening of the density at the H positions in the N—H···O section.

standard deviation in the data set. This procedure eliminates the necessity for a second Lagrangian multiplier in the maximization process. Two sets of density values, $\rho^+(\mathbf{r}_j)$ and $\rho^-(\mathbf{r}_j)$ $(j = 1, M)$, are to be found, which maximize the two-channel entropy, and for which

$$\Delta F_i^{\text{calc}} = (V/M)\sum_{j=1}^{M}[p_j^+ - p_j^-]\exp\{2\pi i\mathbf{H}_i \cdot \mathbf{r}_j\} \qquad (8)$$

fits the ΔF_i^{obs} within the error bars.

3.2. *Uniform vs informative prior model densities*

3.2.1. *Use of uniform models.* Straightforward algebra leads to expressions analogous to (4) for the converged entropic densities:

$$\rho_j^+ = A\exp\{-\lambda[\textstyle\sum(\rho_j^+ + \rho_j^-)]\partial C[\rho]/\partial\rho_j^+\}, \quad j = 1, M$$

and (9*a*)

$$\rho_j^- = A\exp\{-\lambda[\textstyle\sum(\rho_j^+ + \rho_j^-)]\partial C[\rho]/\partial\rho_j^-\}, \quad j = 1, M$$

with

$$A = \exp\left[\sum_{j=1}^{M}(p_j^+ \ln\rho_j^+ + p_j^- \ln\rho_j^-)\right]. \qquad (9b)$$

Since $\partial C[\rho]/\partial\rho_j^+ = -\partial C[\rho]/\partial\rho_j^-$, this gives

$$\rho_j^+\rho_j^- = A^2. \qquad (9c)$$

It follows from (9*a*)–(9*c*) that, in a given pixel $\{\mathbf{r}_j\}$, either ρ_j^+ or ρ_j^- can have a value larger than A, which remains our sensitivity level. The two-channel entropy is now a function of the scale factor k, defined in (5), and will not attain its maximum value unless the spherical part is satisfactorily subtracted out. Consistency requires that $S(k)$ be skewed about the optimal value k_{opt}.

3.2.2. *Use of informative non-uniform models.* When a non-uniform model $\rho_0(\mathbf{r}_j)$ is used as the starting point in the single-channel case, (4*b*) and (4*c*) are replaced by

$$\rho_j/\rho_{0j} = B\exp\{-\lambda(\textstyle\sum\rho_j)\partial C[\rho]/\partial\rho_j\} \qquad (10a)$$

and

$$B = \exp\{\textstyle\sum p_j \ln(\rho_j/\rho_{0j})\}. \qquad (10b)$$

In the particular case of a uniform prior, $\rho_{0j} = \rho_0 =$ constant, B reduces to $B = A/\rho_0$, where $A = \sum p_j \log\rho_j$ is the logarithmic averaged density introduced in §2. Corresponding modifications are made in (9*a*)–(9*c*) for the two-channel method. In particular, (9*c*) is now replaced by

$$\rho_j^+\rho_j^- = B^2\rho_{0j}^+\rho_{0j}^-, \qquad (9d)$$

where

$$B = \exp\{\textstyle\sum[p_j^+ \ln(\rho_j^+/\rho_{0j}^+) + p_j^- \ln(\rho_j^-/\rho_{0j}^-)]\}. \qquad (9e)$$

Note that B is very close to unity when the prior density is very close to the true density. By contrast, it can be substantially different when the prior is vague (*i.e.* uninformative). This is the case for instance when a flat prior is used along with the single-channel method.

The converged entropic density remains insensitive to the initial starting density, but it now depends on the prior density ρ_{0j}. In the extreme case of no experimental data at all, the converged entropic density is the prior density itself. When the experimental data are introduced, the entropic density is the density closest to the prior that fits the data and shows the least amount of spurious correlation.

3.3. *The case of α-glycine at 120 K*

3.3.1. *The scale factor k.* Calculation of the deformation functions defined in (5*a*), (5*b*) requires knowledge of the scale factor k relating the experimental scale to the absolute value of 1 used in the calculation. Since the multipolar model reflects the changes in the electron density due to bonding, the scale factor obtained in the aspherical least-squares refinement is expected to be relatively free from bias due to model inadequacies. We have first rescaled the experimental data with the least-squares scale factor and then tested its validity by searching for deviations from $k = 1$ corresponding to the maximum statistical entropy. The results shown in Fig. 2 indicate agreement to within 1% between the MEM and least-squares scale factors.

3.3.2. *Simulated data set.* The calculated $\Delta F^{\text{multipole}}(\mathbf{H}_k)$ values for 1205 reflections with $\Delta F > 2\sigma(\Delta F)$, with associated standard deviations, were used as a model data set. $\Delta F(000) = 0$ was added as explained in §3.1 to yield a data set consisting of 1206 reflections. O(1)—C(1)—O(2) sections of both the static and dynamic model densities are shown in Fig. 3. It may be noted that the contour interval in the maps (± 0.05 e Å^{-3}) is approximately 40 times less than the sensitivity level used in the total electron-density reconstruction.

The dynamic deformation density $\Delta\rho_{\text{mul}}(\mathbf{r}) = \rho_{\text{mul}}(\mathbf{r}) - \rho_{\text{sph}}(\mathbf{r})$ was reconstructed using (i) the experimental e.s.d. bars and (ii) very small e.s.d. bars about 30

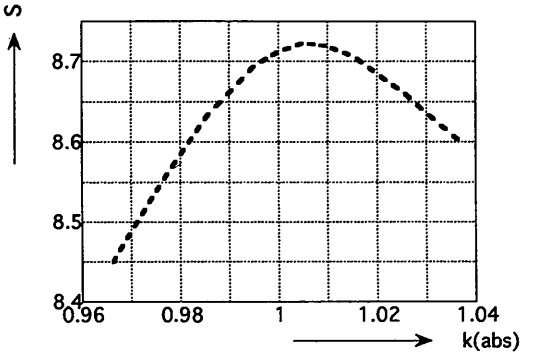

Fig. 2. Entropy as a function of the scale factor k.

times less than the experimental ones. The same default value $A = 0.001\,\text{e}\,\text{Å}^{-3}$ was used in both instances. The O(1)—C(1)—O(2) MEM sections obtained from the simulated $F^{\text{mul}}(\mathbf{H}) - F^{\text{sph}}(\mathbf{H})$ values are shown in Fig. 4. Though the main features are not seriously affected by the variation in the e.s.d. bars, the amount of detail is much larger with the second choice, as expected.

Let us define the total reconstructed density at $\mathbf{r}_j$ as $\rho_j^+ + \rho_j^-$, which is a strictly positive quantity [*cf.* (6) in §3.1]. We find the amount of total reconstructed density numerically integrated over the unit cell to be 2.5 times larger when the smaller error bars are used than when experimental e.s.d. bars are used in the reconstruction. The result in the former case is much closer to the Fourier transform of $F^{\text{mul}}(\mathbf{H}) - F^{\text{sph}}(\mathbf{H})$. The use of experimental e.s.d. bars results in a considerable loss of detail in the reconstruction. We will show below that the lost information is partially recoverable with the use of an informative non-uniform prior.

3.3.3. *MEM with observed data.* The near-optimal value of 1.01 for the scale factor (Fig. 2) is used in the entropic reconstruction with a uniform prior, yielding the

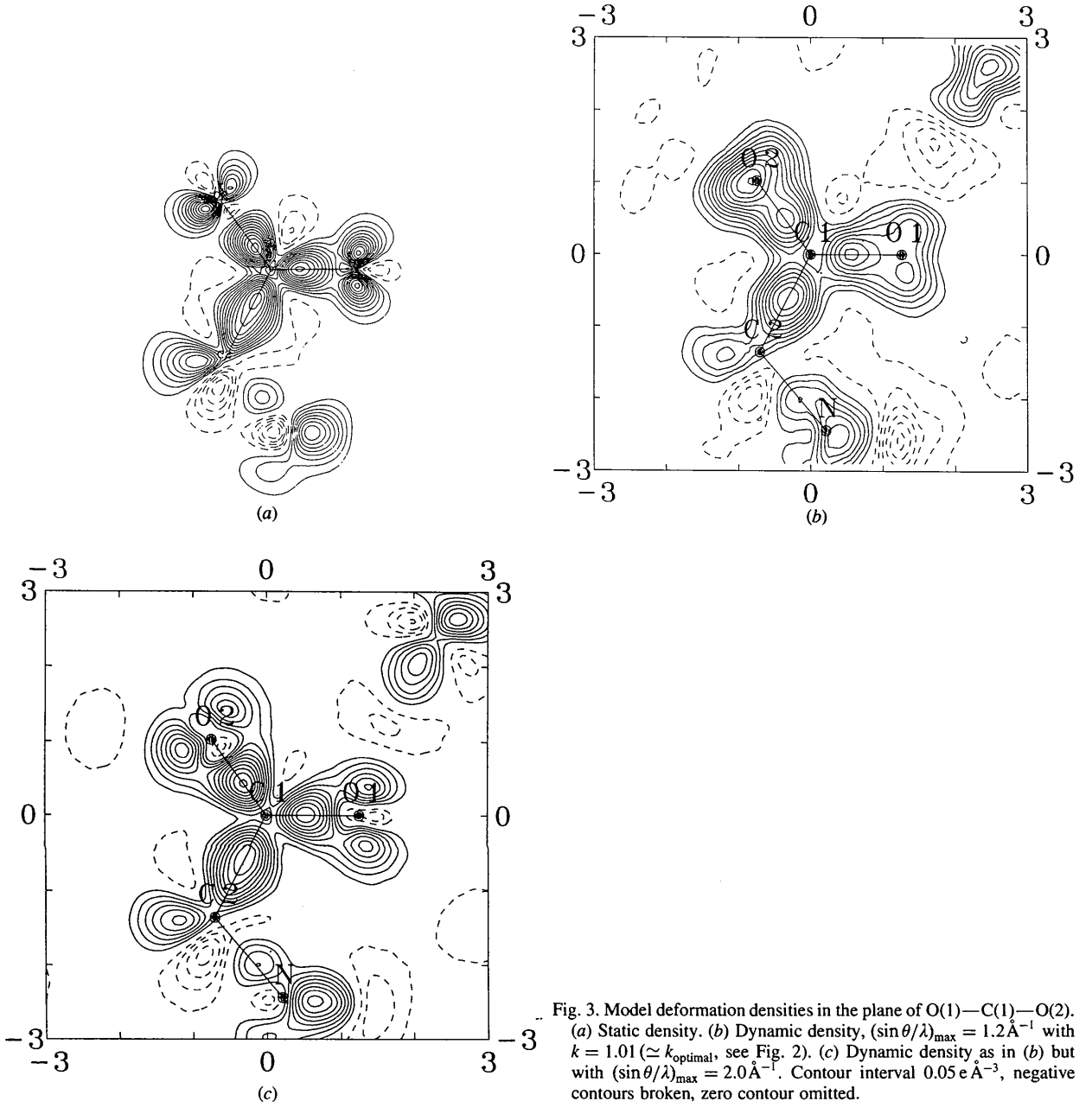

Fig. 3. Model deformation densities in the plane of O(1)—C(1)—O(2). (*a*) Static density. (*b*) Dynamic density, $(\sin\theta/\lambda)_{\text{max}} = 1.2\,\text{Å}^{-1}$ with $k = 1.01\,(\simeq k_{\text{optimal}}$, see Fig. 2). (*c*) Dynamic density as in (*b*) but with $(\sin\theta/\lambda)_{\text{max}} = 2.0\,\text{Å}^{-1}$. Contour interval $0.05\,\text{e}\,\text{Å}^{-3}$, negative contours broken, zero contour omitted.

deformation density $\Delta\rho = 1.01\rho_{obs} - \rho_{sph}$. The MEM densities in the three sections of the molecule previously reported by Legros & Kvick (1980) are compared in Figs. 5, 6 and 7 with the corresponding standard deformation densities obtained directly from the data. It is clear that the use of a uniform prior density sharpens and enhances the bond peaks relative to the observed deformation density but reduces the lone-pair peaks, which are less pronounced in the standard deformation density. Though the main features stand out more clearly in this enhanced deformation density and are sharpened, there is a flattening of the remaining less-prominent features such as the maximum at the back of the N atom in the N—C—C section, in particular when a non-uniform prior is used. This apparent loss of meaningful detail is confirmed by the dipole-moment analysis described in the following section.

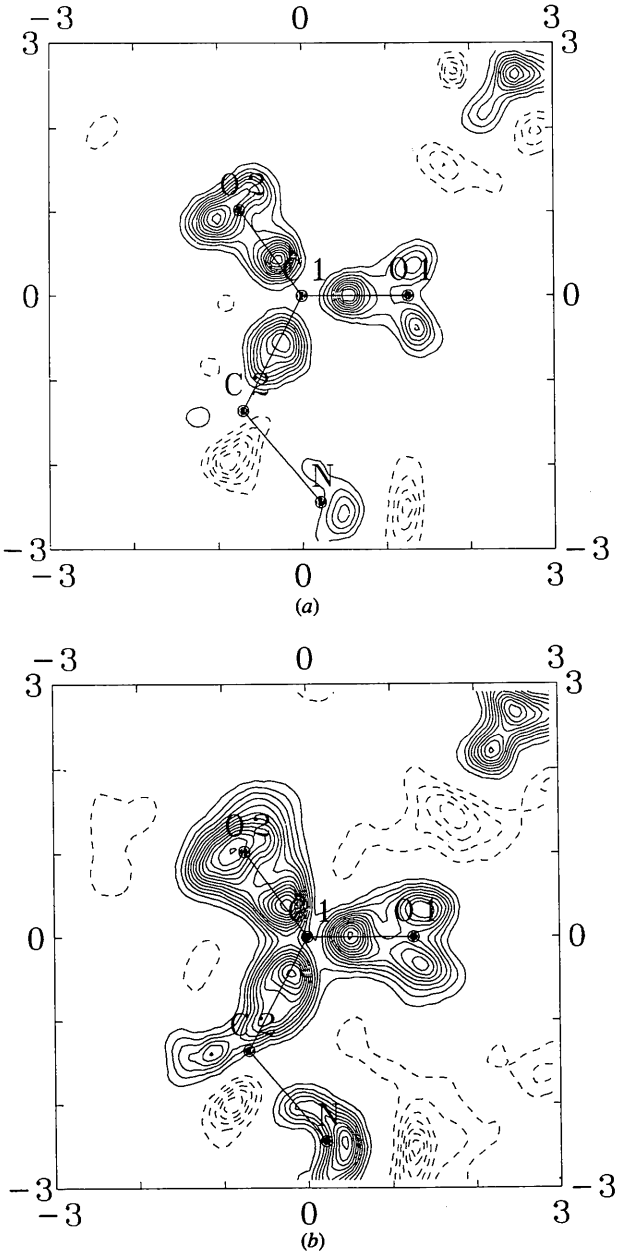

Fig. 4. MEM sections in the O(1)—C(1)—O(2) plane obtained with $F^{mul}(\mathbf{H}) - F^{sph}(\mathbf{H})$ structure amplitudes and a uniform prior. (*a*) Experimental standard deviations. (*b*) Standard deviations reduced by a factor $(1206)^{1/2}$. Contours as in Fig. 3.

Examination of Figs. 5(*b*), 6(*b*) and 7(*b*) shows that the density obtained with a non-uniform prior is preferable. Compared with the density in the corresponding experimental sections (Figs. 5*c*, 6*c* and 7*c*), the non-uniform prior MEM leads to a sharpening of the features in the maps and some increase in detail. An example of the latter is the double maximum in the C—C bond, the significance of which remains to be established. A similar conclusion is reached when the comparison is made with the very high resolution model density of Fig. 3(*c*). The MEM distributions are not restricted by the shape of the model functions, which allow only smooth features to appear in the model maps.

The distribution of the 1206 normalized residuals after the non-uniform prior MEM procedure is shown in Fig. 8.

4. The molecular dipole moment as a test of the MEM procedure

The electrostatic moments, the electrostatic potential, field and the electric field gradient can be extracted from good-quality single-crystal X-ray data (Su & Coppens, 1992). Here, we will use the molecular dipole moment to examine the physical implications of the MEM optimization. An optimization that would produce unrealistic values of the electrostatic properties would obviously not be an acceptable procedure.

The solution value of the dipole moment of the α-glycine molecule is 38.7×10^{-30} C m (Khanarian & Moore, 1980), while our multipole refinement of the Legros & Kvick data gives values of $46.0(14) \times 10^{-30}$ C m when the H nuclei are positioned at the locations from the neutron data (see below) and $39.0(13) \times 10^{-30}$ C m when the H-atom positions from the multipole refinement are used. The former value is to be preferred and suggests a slight increase in dipole moment in the solid state relative to the solution, in agreement with conclusions based on examination of other diffraction-based molecular dipole and quadrupole moments (Spackman, 1992).

The calculation of a dipole moment in direct space from the electron-density distribution requires partitioning of space. A discrete boundary can be based on the partitioning of space into polyhedral volumes, in analogy to Seitz cells used in solid-state science (Coppens, Moss & Hansen, 1980). The method is appropriate for analysis of the MEM densities in that it does not require model

functions, unlike dipole moments derived from the aspherical-atom least-squares refinement.

The boundaries in the discrete boundary space partitioning method are defined by the van der Waals radii of the contacting atoms, a pixel being assigned to the molecule of atom A if $r_A/r_B < R_A/R_B$, r_X and R_X being the distance to atom X and the van der Waals radius of atom X, respectively.

The coordinates of the H atoms at the experimental temperature of 120 K were obtained by interpolation between neutron coordinates from 300 and 20 K measurements (Almlöf, Kvick & Thomas, 1973; Power, Turner & Moore, 1976; Jönsson & Kvick, 1972), assuming contraction of the intermolecular but not intramolecular distances.

Dipole moments for two sets of somewhat different van der Waals radii are listed in Table 1 for both the MEM and the experimental densities. The discrete boundary results from the MEM and experimental densities are directly comparable as

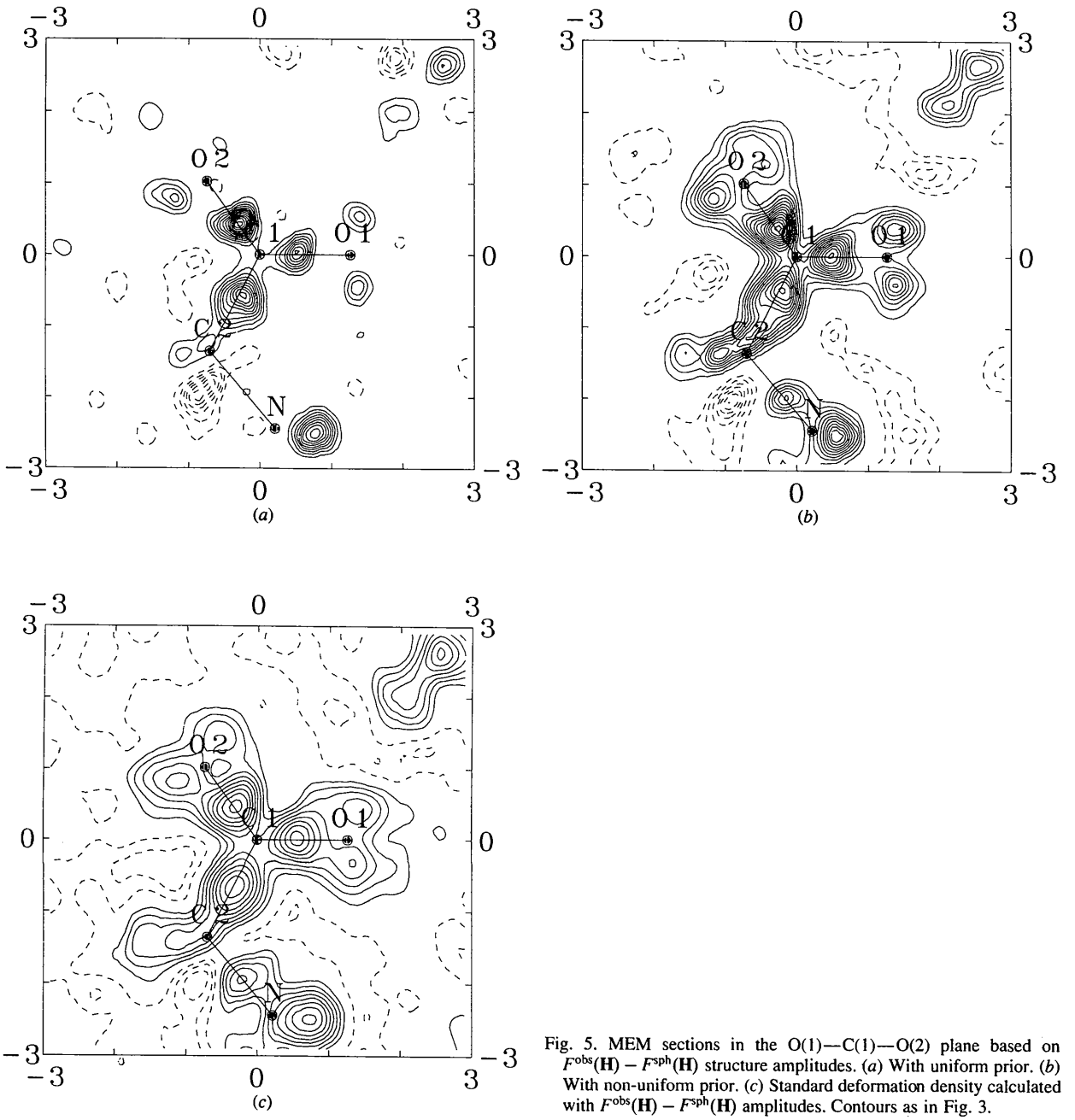

Fig. 5. MEM sections in the O(1)—C(1)—O(2) plane based on $F^{obs}(\mathbf{H}) - F^{sph}(\mathbf{H})$ structure amplitudes. (*a*) With uniform prior. (*b*) With non-uniform prior. (*c*) Standard deformation density calculated with $F^{obs}(\mathbf{H}) - F^{sph}(\mathbf{H})$ amplitudes. Contours as in Fig. 3.

they are based on the same partitioning of space. The uniform prior dipole moment is disappointingly low, while the non-uniform prior result is closer to the experimental value. Nevertheless, remaining discrepancies indicate that physical properties may not be properly preserved in the maximum-entropy procedure.

5. Concluding remarks

Our main focus in this paper has been to explore the optimal way to apply the maximum-entropy method in charge-density studies. We show that a single-channel method is inadequate for the study of detailed bonding features in the electron density. The two-channel method is more successful but does not reproduce the features adequately if a uniform prior density is used. If the information available from the aspherical-atom least-squares refinement is used as a prior density, the MaxEnt method produces reasonable densities, judging from their appearance and the value of the molecular dipole moment. The question whether the MaxEnt method contributes to an increase in information available from the experimental data requires further study. Based on the current results, we cannot make an unequivocal statement in support of the maximum-entropy method in charge-density analysis. It is clear, however, that any further analysis will require a multi- rather than

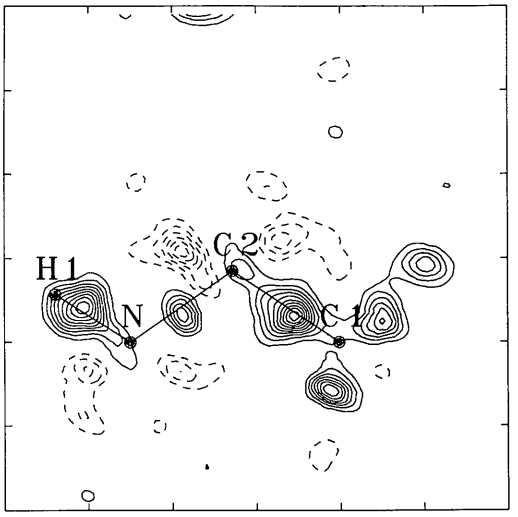

(*a*)

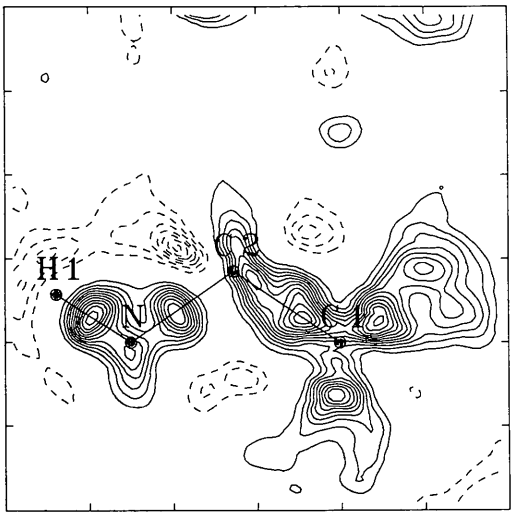

(*b*)

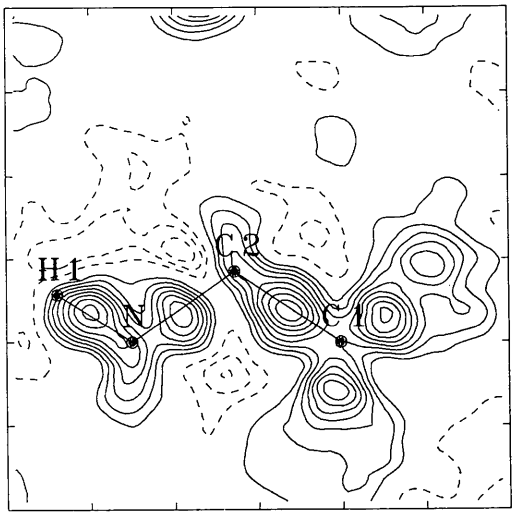

(*c*)

Fig. 6. As Fig. 5 for the N—C(2)—C(1) section. Contours as in Fig. 3.

Table 1. *Molecular dipole moments ($\times 10^{-30}$ C m) from (a) discrete boundary space partitioning and (b) multipole refinement*

	Experimental density (a)		MEM density uniform prior (a)		MEM density non-uniform prior (a)		Multipole model (b)
	Set I	Set II	Set I	Set II	Set I	Set II	
μ_a	2.84	2.20	1.83	1.57	10.77	9.84	16.81
μ_b	−1.00	−1.03	0.47	0.40	−1.87	−1.90	−0.80
μ_c	−29.15	−26.92	−3.40	−3.67	−20.08	−18.8	−31.72
$\lvert\mu\rvert$	30.35	27.79	4.44	4.54	26.15	24.32	46.03 (143)

van der Waals radii used (Å)

	O	N	C	H
Set I:	1.4	1.5	1.7	1.2
Set II:	1.52	1.55	1.65	1.2

a single-channel approach to the reconstruction of the density features.

Finally, it should be mentioned that adoption of the strategy developed in this paper to other problems, such as isotopic substitution (*e.g.* H/D) in neutron diffraction, is straightforward.

The authors thank Dr Å. Kvick for supplying unpublished H-atom parameters, based on a 20 K neutron diffraction study. This work is supported by the National Science Foundation (CHE9317770) and the US Department of Energy under contract no. DE-AC02-76CH-00016.

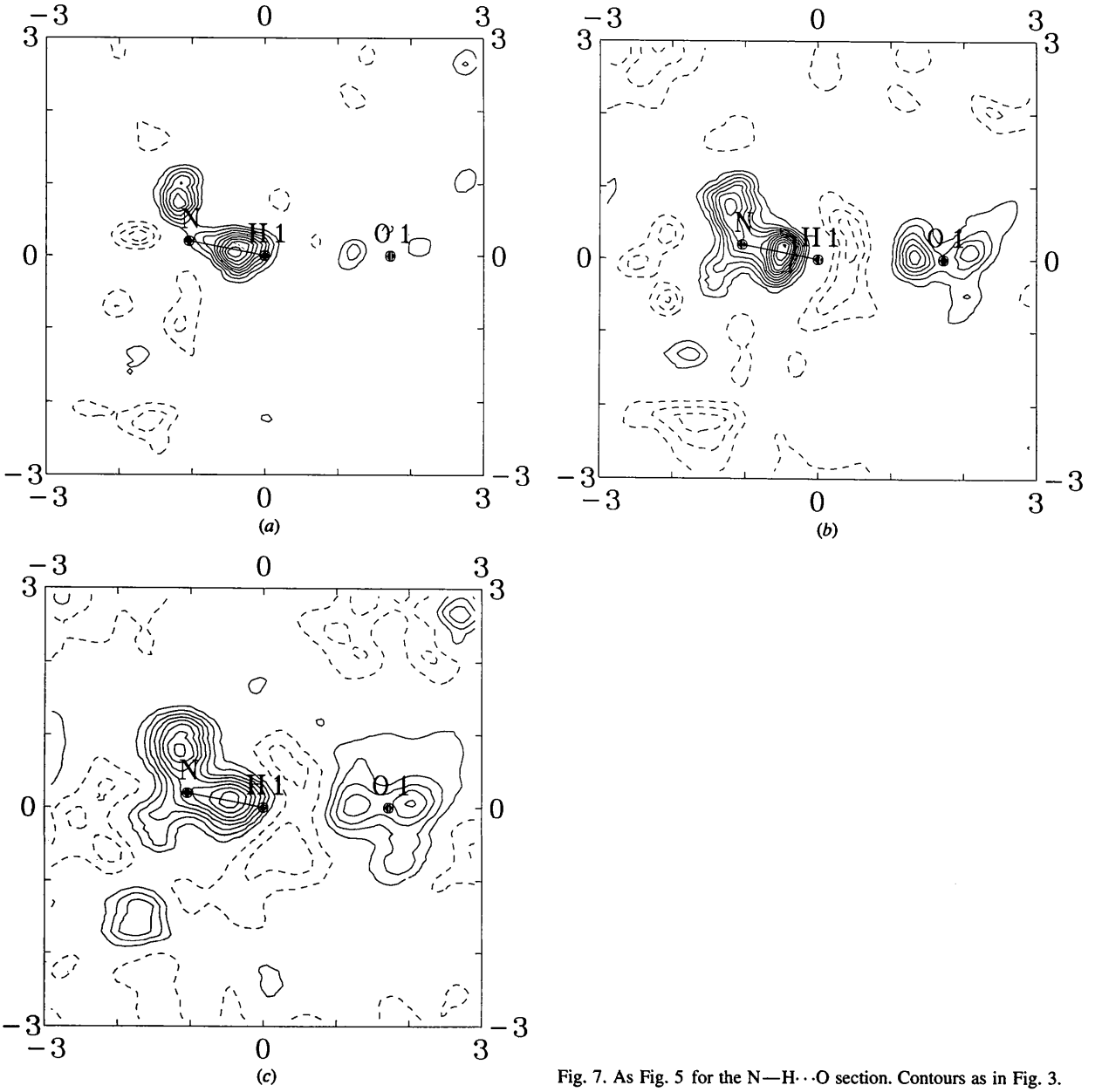

Fig. 7. As Fig. 5 for the N—H···O section. Contours as in Fig. 3.

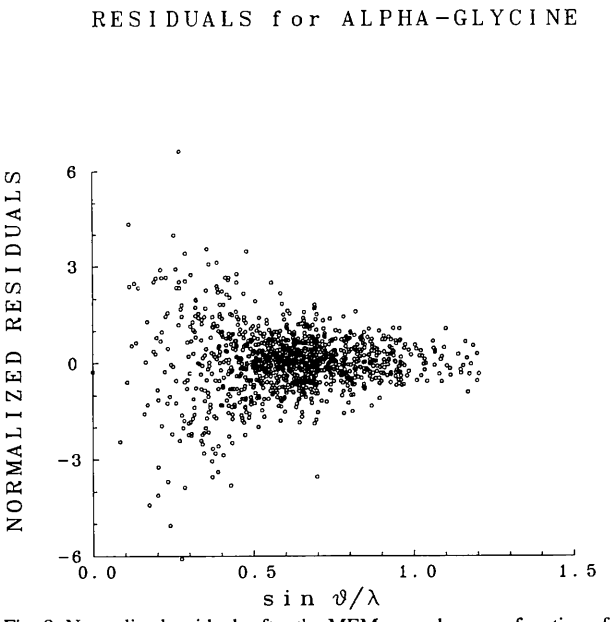

Fig. 8. Normalized residuals after the MEM procedure as a function of $(\sin\theta)/\lambda$ (Å^{-1}). Non-uniform prior density.

References

Almlöf, J., Kvick, Å. & Thomas, J. O. (1973). *J. Phys. Chem.* **59**, 3901–3906.

Bertaut, E. F. (1978). *J. Phys. Chem. Solids*, **39**, 97–102.

Bricogne, G. (1984). *Acta Cryst.* A**40**, 410–445.

Bricogne, G. (1988). *Acta Cryst.* A**44**, 517–545.

Collins, D. M. (1982). *Nature (London)*, **298**, 49–51.

Coppens, P., Moss, G. & Hansen, N. K. (1980). In *Computing in Crystallography*, edited by R. Diamond, S. Ramaseshan & K. Venkatesan, pp. 16.01–16.22. Bangalore: Indian Academy of Sciences.

Frieden, B. R. (1972). *J. Opt. Soc. Am.* **62**, 511–518.

Gull, S. F. & Daniell, G. J. (1978). *Nature (London)*, **272**, 686–690.

Gull, S. F. & Skilling, J. (1991). *MemSys5 User's Manual.* MEDC Ltd, 33 North End, Meldreth, Royston SG8 6NR, England.

Hansen, N. K. & Coppens, P. (1978). *Acta Cryst.* A**34**, 909–921.

Jauch, W. (1994). *Acta Cryst.* A**50**, 650–652.

Jauch, W. & Palmer, A. (1993). *Acta Cryst.* A**49**, 590–591.

Jönsson, D. G. & Kvick, Å. (1972). *Acta Cryst.* B**28**, 1827–1833.

Khanarian, G. & Moore, W. J. (1980). *Austr. J. Chem.* **33**, 1727–1741.

Kumazawa, S., Kubota, Y., Takata, M., Sakata, M. & Ishibashi, Y. (1993). *J. Appl. Cryst.* **26**, 453–457.

Legros, J. & Kvick, Å. (1980). *Acta Cryst.* B**36**, 3052–3059.

Livesey, A. K. & Skilling, J. (1985). *Acta Cryst.* A**41**, 113–122.

Papoular, R. J. (1991). *Acta Cryst.* A**47**, 293–295.

Papoular, R. J. & Gillon, B. (1990*a*). *Europhys. Lett.* **13**, 429–434.

Papoular, R. J. & Gillon, B. (1990*b*). *Neutron Scattering Data Analysis*, edited by M. W. Johnson, *Inst. Phys. Conf. Ser.* No. 107, pp. 101–116.

Papoular, R. J., Prandl, W. & Schiebel, P. (1992). *Maximum Entropy and Bayesian Methods, Seattle, 1991*, edited by C. R. Smith, G. J. Erickson & P. O. Neudorfer, pp. 359–376. Dordrecht: Kluwer.

Power, L. F., Turner, K. E. & Moore, F. H. (1976). *Acta Cryst.* B**32**, 11–16.

Sakata, M. & Sato, M. (1990). *Acta Cryst.* A**46**, 263–270.

Sakata, M., Uno, T., Takata, M. & Howard, C. J. (1993). *J. Appl. Cryst.* **26**, 159–165.

Skilling, J. & Bryan, R. K. (1984). *Mon. Not. R. Astron. Soc.* **211**, 111–124.

Skilling, J. & Gull, S. F. (1985). *Maximum Entropy and Bayesian Methods in Inverse Problems*, edited by C. R. Smith & W. T. Grandy Jr, pp. 83–132. Dordrecht: Reidel.

Spackman, M. A. (1992). *Chem. Rev.* **92**, 1769–1797.

Su, Z. & Coppens, P. (1992). *Acta Cryst.* A**48**, 188–197.